Estimation of liver iron concentration by dual energy CT images: influence of X-ray energy on sensitivity

I. Malvarosa, C. Massaroni, *IEEE Student Member*, C. Liguori, J. Paul, B. Beomonte Zobel, P. Saccomandi, *IEEE Student Member*, T. J. Vogl, S. Silvestri, *IEEE Member,* and E. Schena, *IEEE Member*

Abstract— **In hemochromatosis an abnormal accumulation of iron is present in parenchymal organs and especially in liver. Among the several techniques employed to diagnose the iron overload, magnetic resonance imaging (MRI) and Computed Tomography (CT) are the most promising non-invasive ones. MRI is largely used but shows limitation including an overestimation of iron and inability to quantify iron at very high concentrations. Therefore, some research groups are focusing on the estimation of iron concentration by CT images. Single X-ray CTs are not able to accurately perform this task in case of the presence of confounding factors (e.g., fat). A potential solution to overcome this concern is the employment of Dual-Energy CT (DECT).**

The aim of this work is to investigate influence of the kVp and mAs on CT number sensitivity to iron concentration. A phantom with test tubes filled with homogenized porcine liver at different iron concentrations, has been scanned with DECT at different mAs. The images have been analyzed using an ad-hoc developed algorithm which allows minimizing the influence of air bubbles present in the homogenized. Data show that the sensitivity is strongly influenced by kVp (its value almost halves from 80 kVp to 140 kVp; e.g. 0.41 g·µmol^{-1} and 0.19 g·µmol^{-1} at 80 kVp/120 mAs and 140 kVp/60 mAs respectively), on the other hand the influence of mAs value is negligible.

I. Introduction

Iron is an essential micronutrient that is a critical component of oxygen transport proteins (hemoglobin and myoglobin) and of numerous enzymes. Nevertheless iron excess in vital organs causes organ failure. In hemochromatosis or other genetic disorders leading to an impaired synthesis of globin chains as Thalassemias disorders, iron can build up in most of body's organs, but especially in the liver, heart, and pancreas. Too much iron in the liver can cause an enlarged liver, failure, cancer, or cirrhosis [1]. If iron overload is not treated, it may even cause death.

The estimation of iron concentration in the liver can be carried out through invasive or non-invasive techniques. The most reliable method to calculate iron amount within organs is histochemical or biochemical assessment using a liver biopsy specimen [2]. The need of patient hospitalization and the high cost are the main drawbacks of these analyses. Therefore, several non-invasive procedures have been pursued. Among others, magnetic resonance imaging (MRI) using T2* gradient echo technique has proven to be a promising method to assess iron content in liver [3,4]; furthermore, recently it is also employed to assess cardiac functional parameters [5,6]. However, MRI tends to overestimate the iron concentration due to its magnetic field [7] and shows an inability to quantify iron concentration above 300 µmol/g [8].

An alternative technique to estimate iron overload is based on computed Tomography (CT) images. Quite short duration and low costs of CT examinations suggest to use CT rather than MRI scanner. The estimation of iron concentration by CT scan images is based on the attenuation coefficient of the iron which is much higher than the one of the soft tissues. Single X-ray is used in many medical applications [9,10,11], but CT is not sufficient to accurately estimate the liver iron concentration due to the co-existence of fat. The fat tissues exhibit a low CT attenuation coefficient than the normal liver tissues; hence, it inversely affects the CT numbers [11]. Therefore, dual-energy CT (DECT) was employed for the quantification of liver iron since 1980s [12], due to the application of two different X-ray tube voltages (e.g., 80 kVp and 140 kVp). Moreover DECT allows to get data about iron liver concentration with a broad spatial distribution respect to biopsy. Despite of the higher dose exposure, the added value of DECT has been largely demonstrated [13].

The main aim of this work is to investigate the influence of CT settings (i.e., kVp and mAs) on CT number sensitivity to iron concentration. In order to perform this study a phantom, containing 11 test tubes filled with homogenized liver tissue at different concentrations of iron, has been prepared and scanned with DECT. Since the presence of small air bubbles within the test tubes, a simple algorithm has been developed in Matlab® environment in order to remove the pixels of the images representing with the air bubbles.

I. Malvarosa, C. Massaroni, P. Saccomandi, S. Silvestri and E. Schena are with the Unit of Measurements and Biomedical Instrumentation, Center for Integrated Research, Università Campus Bio-Medico di Roma, Via Álvaro del Portillo, 21-00128- Rome-Italy (e-mail: ilaria.malvarosa@alice.it; c.massaroni, p.saccomandi, s.silvestri, e.schena {@unicampus.it}).

B. Beomonte Zobel is with the Unit of Radiology, Università Campus Bio-Medico di Roma, Via Álvaro del Portillo, 21-00128- Rome-Italy (e-mail: b.zobel@unicampus.it.

C. Liguori is with the Unit of Radiology, AORN Cardarelli, Naples-Italy (e-mail: carlo.liguori@gmail.it.)

J. Paul and T. Vogl are with the Institute of Diagnostic and Interventional Radiology, Goethe University, Theodor-Stern-Kai,7-60590-Frankfurt am Main, Germany (email: Jijopaul1980@gmail.com, T.Vogl@em.uni-frankfurt.de).

978-1-4244-7929-0/14/$26.00 ©2014 IEEE

II. Theoretical Background

A CT scan image consists of a matrix of pixels, representing the average X-ray attenuation profile of the tissue in the corresponding voxel.

Voxels raw data are processed to obtain an attenuation value for each pixel of the final reconstructed image, the *CT number*, expressed in dimensionless Hounsfield Units (HU):

$$CT(x,y) = 1000 \frac{[\mu(x,y) - \mu_{H2O}]}{\mu_{H2O}} \qquad (1)$$

where μ_{H2O} is the linear attenuation coefficient of water, and $\mu(x,y)$ is the average linear attenuation coefficient corresponding to the (x,y) pixel.

Photoelectric absorption is highly dependent on photon energy and the atomic number (Z) of the absorber. At low photon energies, the photoelectric effect dominates the attenuation processes in soft tissue (low Z); when higher energy photons (i.e., higher than 75 keV) interact with low Z materials, Compton scattering dominates [14]. In this range of photon energy, the energy loss due to these processes is proportional to electronic density, $\rho_e = NZ/A$, where A and Z are the atomic mass and atomic number respectively, and N is Avogadro's number. The value of ρ_e varies with physical density (mass, M, per unit of volume, V) for a given material, ρ, whose dependence on linear attenuation coefficient μ can be written as follows:

$$\mu(\rho) = \mu_m \cdot \rho \qquad (2)$$

being μ_m the mass attenuation coefficient of the material.

Due to the strong difference between the soft tissue density and the iron, the amount of iron within the liver influences the liver absorption coefficient: the higher is the iron concentration, the higher is this absorption coefficient, hence the CT number.

The estimation of liver iron concentration can fails with the presence of fat, which causes a decrease of the attenuation coefficient by lowering the CT numbers [15]. In order to overcome this problem, a potential solution is the employment of Dual-Energy CT (DECT). It uses two rotating X-ray tubes with two different voltages applied across these tubes and an automatic dose modulation protocol adjusts the tube current to maintain image noise at the optimal level. Since the attenuation coefficient strongly depends on the X-ray energy, which depends on the voltage applied across the tube, each image acquired is energy dependent. The changes in attenuation at different X-ray spectra can help to differentiate different materials.

III. Phantom Preparation and Experimental Set Up

A. Phantom

Different amounts of ferric nitrate in its nonahydrate form $Fe(NO_3)_3 \cdot 9H_2O$ were added to homogenized porcine liver, in order to obtain 11 solutions with the following concentrations: 0, 20, 40, 60, 80, 100, 120, 160, 180, 200, and 300 µmol/g. The liver has been soaked in physiological solution aiming to keep it in stable isotonic conditions at 4 °C for 3 hours; the soaking was repeated three times intervals of three hours. Then the liver was let dried out through a tissue paper at 4°C for 12 hours. Afterwards, the dry liver was homogenized with a common cooking mixer (BRAUN Multiquick 3, Braun GmbH). Lastly, 11 test tubes were filled with 20 mL of liver at the aforementioned different concentrations. Each solution was remixed to be as homogeneous as possible and was compressed to minimize the presence of air bubbles. The phantom consisted of 11 test tubes placed in a polystyrene box.

B. Experimental set up and CT settings

The phantom examination was performed using a DECT imaging unit (SOMATOM Definition Flash, Siemens Healthcare, Germany). Scans were carried out using a tube voltage pair of 80kV and 140kV (with tin filter) and setting three different mAs values for each tube. Thus three different phantom protocols were performed: protocol 1 (80 kV with 120 mAs and 140 kV with 60 mAs), protocol 2 (80 kV with 201 mAs and 140 kV with 99 mAs) and protocol 3 (80 kV with 250 mAs and 140 kV with 125 mAs). The slice thickness was 0.6 mm and the images were reconstructed using a soft kernel (D30f).

During post processing, fused image data were obtained using five different weighting factors: 0.0, 0.2, 0.5, 0.8 and 1.0. The weighting factors correspond to the percentage contribution of image information derived from 80 and 140kVp data [16]. A custom-made algorithm, developed in Matlab® environment, allows selecting the pixels of the test tubes contained in a polygonal ROI, and excluded the ones lower than a threshold value of -120 HU. This method aims to minimize the influence of air bubbles within the homogenized liver on the ROI-averaged CT number (Fig. 1). Since the CT number of the main components of liver tissue (fat, water and soft tissues) are higher than -120 HU [17], the threshold allows excluding only the pixels containing air bubbles. Therefore, the proposed algorithm avoids the underestimation of averaged CT number of the filled test tubes caused by the presence of the air bubbles; moreover, it entails a decrease of the CT number standard deviation of the selected ROI because excludes the pixels that can be considered outliers. Therefore, the analyses concerning the relationship between the CT number and the iron concentration have been performed on the data obtained by applying the aforementioned algorithm.

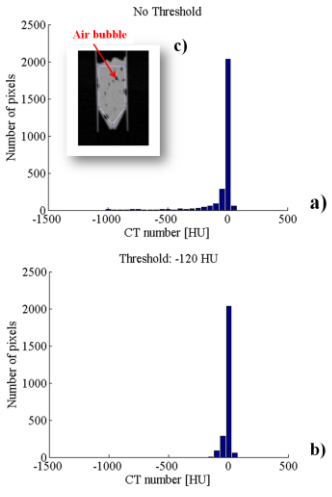

Figure 1. Pixels histogram of a polygonal ROI without the threshold (a) and with the threshold (b); c) Example of a tes tube with air bubbles.

IV. Results and Discussion

The mean CT number of the pixels contained within the ROIs representing each test tube has been calculated and represented as a function of iron concentration. This calculation has been performed considering the images obtained by each protocol and the five different weighting factors. Lastly, the best fitting lines has been calculated for each protocol.

Figure 2 shows the averaged CT number as a function of iron concentration and the best fitting lines obtained by the protocol 1 and the five weighting factors.

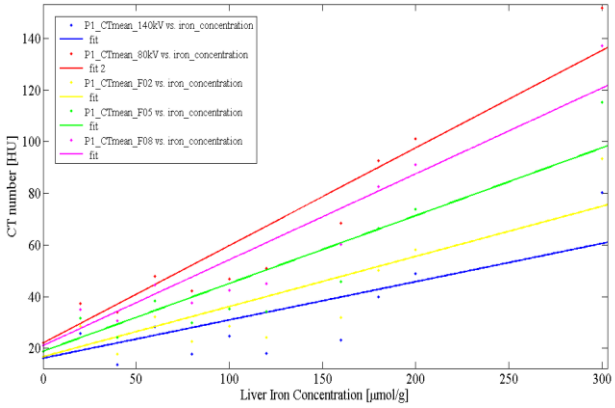

Figure 2. Comparison of CT measurements *vs* iron concentration at the five weighting factors for the protocol 1. Experimental data and best fitting line at weigthing factor 1.0 (red), 0.8 (pink), 0.5 (green), 0.2 (yellow) and 0.0 (blue).

Figures 3 and 4 show the averaged CT number as a function of iron concentration and the best fitting lines obtained by the protocol 2 and the protocol 3 respectively at the five weighting factors.

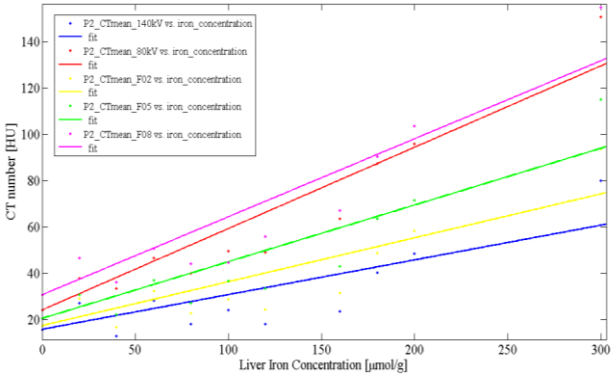

Figure 3. Comparison of CT measurements vs iron concentration at the five weighting factors for the protocol 2. . Experimental data and best fitting line for weigthing factor 1.0 (red), 0.8 (pink), 0.5 (green), 0.2 (yellow) and 0.0 (blue).

The linearity of the relationship between CT number and iron concentration is confirmed by the high value of the correlation coefficient for all the protocols.

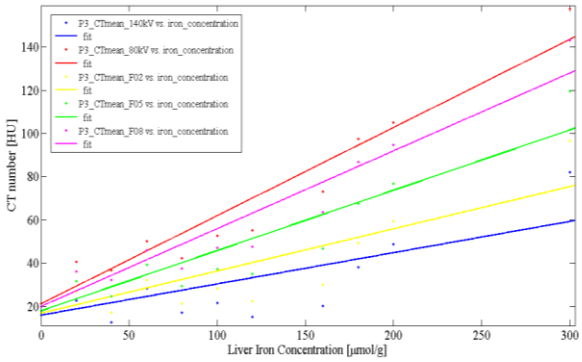

Figure 4. Comparison of CT measurements vs iron concentration at the five weighting factors for the protocol 3. Experimental data and best fitting line for weigthing factor 1.0 (red), 0.8 (pink), 0.5 (green), 0.2 (yellow) and 0.0 (blue).

The slopes of the best fitting lines represent the sensitivity of CT number to iron concentration. Table I shows the sensitivities for the three protocols and considering the spectral (both 80 kVp and 140 kVp) and weighted data.

TABLE I. Correlation coefficient (R) and Sensitivity (S) at the different protocols

	R			***S [g·µmol^{-1}]***		
Protocol	***1***	***2***	***3***	***1***	***2***	***3***
80 kVp	0.97	0.96	0.97	0.41	0.39	0.43
F_0.8	0.96	0.95	0.96	0.36	0.39	0.39
F_0.5	0.94	0.93	0.94	0.30	0.29	0.31
F_0.2	0.90	0.89	0.89	0.23	0.23	0.24
140 kVp	0.86	0.86	0.84	0.19	0.19	0.19

Data analysis shows that the sensitivity is strongly influenced by the kVp and the weighting factor. Indeed, the higher is the kVp, the lower is the sensitivity: for instance, at the protocol 1 the sensitivities are 0.41 g·µmol^{-1} and 0.19 g·µmol^{-1} respectively for 80 and 140 kV data. This result agrees with data reported by Fischer et al. [13], which show a good linearity between CT number and iron concentration up to 800 µmol·g^{-1} and the sensitivity decreases with kVp increasing. On the other hand, the value of mAs does not influence sensitivity, as clearly shown in Table I. Therefore, the highest sensitivity is obtained at 80 kVp and 250 mAs (protocol 3). The use of setting with high sensitivity can result crucial to discriminate iron concentration lower than the threshold defining hepatic iron overload (36 µmol·g^{-1}) [16]. For instance, at 80 kVp the marked difference of Hounsfield unit (i.e., 20 HU) between the test tube without iron and the one with 20 µmol·g^{-1} (see Fig. 2–4) allows discriminating the two different concentrations.

On the other hand, the employment of fused images can be useful to minimize the influence of confounding factor. Therefore, the use of fused images with weighting factor of 0.8 might be recommended to minimize the influence of confounding factor avoiding an excessive decrease of sensitivity.

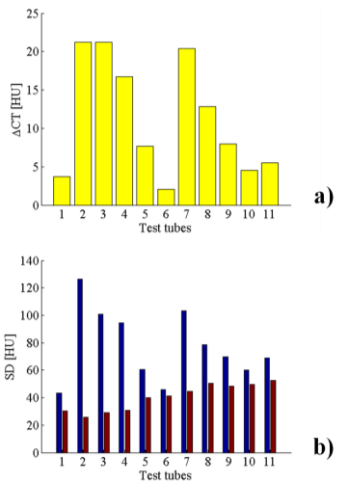

Figure 5. a) Differences of averaged CT number calculated in the same ROI (testing tube at 80 kVp and 120 mAs) with and wihout the threshold at -120 HU; b) differences of standard deviation with (red bars) and wihout (blue bars) the threshold.

Lastly the attention has been focused on the importance of employing the algorithm based on the threshold at -120 HU. It allows avoiding underestimation of the mean CT number (e.g. underestimation ranged from 2 HU up to 21 HU); moreover, it entails a decrease of the CT number standard deviation of the selected ROI (e.g. decrease ranged from 5 HU up to 101 HU).

V. Conclusion

This study presents how the CT scan settings (mAs and kVp) influences the Hounsfield unit sensitivity to iron concentration. The experiments were performed using a DECT an ad hoc designed phantom, containing 11 test tubes filled with homogenized liver at different iron concentrations. The scans were performed at three different protocols and the analysis was carried out using fused images obtained at five different weighting factors. The iron concentrations covered a range of values much wider than the one encountered in condition of iron overload.

The relationship between the CT number and the concentration shows good linearity at all the protocols. The sensitivity of the Hounsfield unit to iron is strongly influenced by kVp, on the other hand the influence of mAs value is negligible.

This analysis might be useful to assess the ability of DECT-based approach in discriminating concentrations lower than 36 $\mu mol \cdot g^{-1}$, which is considered the threshold defining hepatic iron overload [18].

Our ex vivo study shows that the method is able to discriminate concentration lower than the mentioned threshold: at the settings with high sensitivity, test tube with 20 $\mu mol \cdot g^{-1}$ of concentration has a Hounsfield unit higher than the one without adding iron. Obviously, our results inherent to an ex vivo study might not be generalizable to patients with the same accuracy.

Further trials might be performed in order to analyze the discrimination threshold of the proposed technique on patients and to compare results obtained by DECT images and by MRI.

References

[1] PT Telfer, E Prestcott, S Holden, M Walker, AV Hoffbrand, and B Wonke, “Hepatic iron concentration combined with long-term monitoring of serum ferritin to predict complications of iron overload in thalassaemia major”, *Br J Haematol*, vol. 110, pp. 971–977, 2000.

[2] M Barry and S Sherlock S, “Measurement of liver-iron concentration in needle-biopsy specimens”, *Lancet*, vol.1, pp.100-103, 1971.

[3] M Bydder, M Shiehmorteza, Yokoo T et al, “Assessment of liver fat quantification in the presence of iron”, *Magn Reson Imaging*, vol. 28, pp. 767–776, 2010.

[4] Y Gandon, D Olivié, D Guyader, C Aubé, F Oberti, V Sebille, Y Deugnier, “Non-invasive assessment of hepatic iron stores by MRI”, *Lancet*, vol. 363, pp. 357-362, 2004.

[5] C Liguori, F Pitocco, I Di Giampietro, A De Vivo, E Schena, P Cianciulli, and B Beomonte Zobel, “Relationship between myocardial T2* values and cardiac volumetric and functional parameters in β-thalassemia patients evaluated by cardiac magnetic resonance in association with serum ferritin levels”, *Euro J Radiol*, Vol. 82, pp. e441-e447, 2013.

[6] C Liguori, I Di Giampietro, F Pitocco, A De Vivo, E Schena, L Mortato, F Pirro, P Cianciulli, and B Beomonte Zobel, “Dark blood versus bright blood T2* acquisition in cardiovascular magnetic resonance (CMR) for thalassaemia major (TM) patients: Evaluation of feasibility, reproducibility and image quality”, *Euro J Radiol*, Vol. 83, pp. e8-e14, 2014

[7] A Castiella, JM Alústiza, JI Emparanza, EM Zapata, B Costero, MI Díez, “Liver iron concentration quantification by MRI: are recommended protocols accurate enough for clinical practice?”, *Eur J Radiol*, vol. 21, pp. 137–141, 2011.

[8] Gandon Y, Guyader D, Heautot JF, Reda MI, Yaouanq J, Buhé T, Brissot P, Carsin M, Deugnier Y, “Hemochromatosis: diagnosis and quantification of liver iron with gradient-echo MR imaging.”, *Radiology*, vol. 193, pp. 533–538, 1994.

[9] E. Schena, P. Saccomandi, F. Giurazza, M.A. Caponero, L. Mortato, F.M. Di Matteo, F. Panzera, R. Del Vescovo, B. Beomonte Zobel, S. Silvestri, “Experimental assessment of CT-based thermometry during laser ablation of porcine pancreas”, *Phys Med Biol*, vol. 58 (16), pp. 5705-5716, 2013.

[10] E. Schena, P. Saccomandi, F. Giurazza, R. Del Vescovo, L. Mortato, M. Martino, F. Panzera, F.M. Di Matteo, B. Beomonte Zobel, S. Silvestri, “Monitoring of temperature increase and tissue vaporization during laser interstitial thermotherapy of ex vivo swine liver by computed tomography”, *Proc 35th Annu. International Conf. IEEE Eng Med Biol Soc*, Osaka, 2013, pp. 378-381.

[11] Boll DT, Merkle EM, “Diffuse liver disease: strategies for hepatic CT and MR imaging”, *Radiographics,* vol. 29, pp.1591–1614, 2009.

[12] Goldberg HI, Cann CE, Moss AA, Ohto M, Brito A, Federle M, “Noninvasive quantitation of liver iron in dogs with hemochromatosis using dual-energy CT scanning”, *Invest Radiol*, vol. 17, pp. 375–380, 1982.

[13] Fischer MA, Reiner CS, Raptis D, Donati O, Goetti R, Clavien PA, Alkadhi H, “Quantification of liver iron content with CT-added value of dual-energy”, *Eur Radiol*, vol. 21, pp. 1727–1732, 2011.

[14] JT Bushberg, JA Seibert, EM Leidholdt, JM Boone, *The essential physics of medical imaging*, 2nd ed., JT Bushberg, New York: Lippincott Williams & Wilkins, pp. 327–369, 2011.

[15] Boll DT, and Merkle EM, "Diffuse liver disease: strategies for hepatic CT and MR imaging", *Radiographics,* vol. 29, pp. 1591-1614, 2009.

[16] J Paul, RW Bauer, W Mäntele and TJ Vogl, "Image fusion in dual energy computed tomography for detection of various anatomic structures – Effect on contrast enhancement, contrast-to-noise ratio,signal-to-noise ratio and image qualitiy", *Eur J Radiol*, vol. 80, pp. 612-19, 2011.

[17] TRC Johnson, B Krauss, M Sedlmair, M Grasruck, H Bruder, D Morhard et al., “Material differentiation by dual energy CT: initial experience”, *Eur Radiol*, vol. 17, pp. 1510-1517, 2007.

[18] A Pietrangelo,” Hereditary hemochromatosis: pathogenesis, diagnosis, and treatment”, *Gastroenterology*, vol. 139, pp. 393–408, 2010.